6-2016

Can Significant Trends be Detected in Surface Air Temperature and Precipitation Over South America in Recent Decades?

Daniel de Barros Soares
University of California, Los Angeles

Huikyo Lee
NASA Jet Propulsion Laboratory

Paul C. Loikith
Portland State University, ploikith@pdx.edu

Armineh Barkhordarian
University of California, Los Angeles

Carlos R. Mechoso
University of California, Los Angeles

Citation Details

de Barros Soares, D., Lee, H., Loikith, P. C., Barkhordarian, A. and Mechoso, C. R. (2017), Can significant trends be detected in surface air temperature and precipitation over South America in recent decades?. Int. J. Climatol., 37: 1483–1493.

INTERNATIONAL JOURNAL OF CLIMATOLOGY
Int. J. Climatol. **37**: 1483–1493 (2017)
Published online 15 June 2016 in Wiley Online Library
(wileyonlinelibrary.com) DOI: 10.1002/joc.4792

RMetS
Royal Meteorological Society

Can significant trends be detected in surface air temperature and precipitation over South America in recent decades?

Daniel de Barros Soares,[a,b] Huikyo Lee,[c] Paul C. Loikith,[d]* Armineh Barkhordarian[a] and Carlos R. Mechoso[a]

[a] *Department of Atmospheric and Oceanic Sciences, University of California Los Angeles, CA, USA*
[b] *Ecole Polytechnique, Palaiseau, France*
[c] *Jet Propulsion Laboratory, California Institute of Technology, Pasadena, CA, USA*
[d] *Department of Geography, Portland State University, OR, USA*

ABSTRACT: Trends in near-surface air temperature and precipitation over South America are examined for the periods 1975–2004 and 1955–2004, respectively, using multiple observational and climate model data sets. The results for observed near-surface air temperature show an overall warming trend over much of the continent, with the largest magnitudes over central Brazil. These observed trends are found to be statistically significant using pre-industrial control simulations from the fifth phase of the Coupled Model Intercomparison Project (CMIP5) as the baseline to estimate natural climate variability. The observed trends are compared with those obtained in natural-only CMIP5 simulations, in which only natural forcings (i.e. volcanoes and solar variability) are included, and in historical CMIP5 simulations, in which anthropogenic forcings (i.e. changes in the atmospheric composition) are further incorporated. The historical CMIP5 simulations are more successful in capturing the observed temperature trends than the simulations with natural forcings only. It is suggested that anthropogenic warming is already evident over much of South America. Unlike the warming trends, observed precipitation trends over South America are less spatially coherent with both negative and positive values across the continent. Significant positive trends are found over South America in only one of the data sets used, and over a region that roughly encompasses the southern part of La Plata Basin (southern Brazil, Uruguay, and northeastern Argentina) in all data sets used. The historical CMIP5 simulations do not capture this feature. No firm conclusions are reached, therefore, for anthropogenic influences on precipitation changes in the period selected for study.

KEY WORDS temperature trends; precipitation trends; South America; CMIP5 models

Received 11 December 2015; Revised 1 April 2016; Accepted 4 May 2016

1. Introduction

Anthropogenic influences on climate change at the global scales have been detected with high confidence in near-surface air temperature (SAT) and less certainty in precipitation (IPCC, 2013). SAT has increased over most of the globe over the last several decades, whereas the magnitude and even sign of precipitation trends can vary regionally (Zhang *et al.*, 2006). The detection of trends at regional scales is particularly challenging because of the general reduction in signal-to-noise ratio with decreasing area of aggregation (Zwiers and Zhang, 2003).

This study aims to provide a quantitative identification of trends in temperature and precipitation over South America during the periods 1975–2004 and 1955–2004, respectively. South America is a geographically complex region. The continent extends meridionally from roughly 15°N to 60°S and encompasses a variety of ecosystems and climate zones. The climate in some regions can be highly influenced through teleconnections by sea surface temperature (SST) variability at several time scales in the Pacific, Atlantic, and even the Indian Oceans. Examples of relevant modes of SST variability are the El Niño Southern Oscillation (Ropelewski and Halpert, 1987; Mechoso and Iribarren, 1992; Robertson and Mechoso, 1998), the Pacific Decadal Oscillation (Mantua and Hare, 2002; Kayano and Andreoli, 2007), and the Atlantic Multidecadal Oscillation (Knight *et al.*, 2006). Influential geographical features on South America's climate include the Andes Mountains (a major coastal range with the highest proportion of the world's tropical glaciers), Amazon rainforest (the biggest tropical forest of the planet), Pantanal wetlands (the largest wetlands in the world), and the first and fifth largest river basins in the world (Amazon and La Plata, respectively).

According to the Working Group I contribution to the Fifth Assessment Report (AR5) of the Intergovernmental Panel on Climate Change (Magrin *et al.*, 2014), SAT over South America has been increasing over the last several decades, coincident with the retreat of tropical glaciers (area loss between 20 and 50%; Bradley *et al.*, 2009). In contrast, precipitation changes during the period have considerable geographical variations and are

* Correspondence to: P. C. Loikith, Department of Geography, PO Box 751 - GEOG, Portland State University, Portland, OR 97207-0751, USA.
E-mail: ploikith@pdx.edu

highly influenced by SST variability. Espinoza Villar *et al.* (2009) found that mean rainfall in the Amazon basin has decreased in 1964–2003. This decrease had stronger amplitude after 1982, especially in the Peruvian western Amazon (Lavado Casimiro *et al.*, 2012), where convection and cloudiness have also decreased (Arias *et al.*, 2011). Precipitation increases have been detected in southeastern South America and northwest Peru. Additional precipitation decreases have been documented in southwest Argentina and southern Peru since 1960. Northeast Brazil (NEB) has experienced a slight decrease in rainfall since the 1970s (Marengo *et al.*, 2013). It has been reported that the dry-season length over South America has increased significantly since 1979, and this feature has been associated with a poleward shift of the southern subtropical westerly jet (Fu *et al.*, 2013). The global climate models contributing to the fifth phase of the Coupled Model Intercomparison Project (CMIP5; Taylor *et al.*, 2012) project a robust increase in SAT across the entire continent by the end of the 21st century. In contrast, the models project an overall decrease in precipitation over subtropical dry belts and an overall increase in precipitation over the Tropics and mid to high latitudes by the end of the 21st century (Knutti and Sedlacek, 2013).

In addition to natural climate variability, variations in the composition of the atmosphere – and associated radiative forcing – due to anthropogenic activities may contribute to temperature and precipitation changes over South America. Another major driver of climate change over the continent is land-use changes due to expanding agricultural activities and aerosols from biomass burning. In fact, land use and land cover changes are believed to contribute approximately 20% of the current anthropogenic CO_2 emissions (Meyer and Turner, 1994). Doyle and Barros (2011) indicate that increased streamflow of major rivers in southeastern South America has been associated with an increase in precipitation and a reduction in evapotranspiration from land-use changes. Such changes also have implications for climate change on a global scale. Exbrayat and Williams (2015), for example, suggest that biomass loss due to deforestation in the Amazon alone has contributed approximately 1.5% of the recent increase in atmospheric CO_2.

This study goes beyond previous analyses of trends in temperature and precipitation over the region. Firstly, we use multiple observational data sets, taking uncertainties across different records into consideration. Secondly, we estimate uncertainty of the observed trends using 'natural variability' obtained from pre-industrial control simulations in CMIP5. The observed trends obtain statistical robustness if they are stronger than the estimated level of natural variability. Lastly, we compare the trends obtained using observational data with those calculated from two different experiments in CMIP5: (1) simulations with natural-only forcings (i.e. volcanoes and solar variability) and (2) simulations with both natural and anthropogenic forcings (historical runs). Based on this quantitative comparison between observed and simulated trends considering natural variability, we will suggest that observed trends, particularly in SAT, can be better reproduced by models only when both natural and anthropogenic forcings are included.

The remainder of this article is organized as follows. In Section 2, we discuss the observational data sets used, the data from CMIP5 models, and the methodology adopted. Sections 3 and 4 present the results including the detection of observed trends in SAT and precipitation, quantification of uncertainty in the observed trends, and comparison between observed and simulated trends. In Section 5, the main conclusions and a discussion are presented.

2. Data sets and methods

The period chosen for study of SAT is 1975–2004. Barkhordarian *et al.* (2012) analysed climate change over the Mediterranean region for the same period. For precipitation, a longer period of 1955–2004 was selected because its temporal and spatial variability are stronger than for SAT. The ending year of 2004 was chosen as to allow for comparison of observed trends with CMIP5 historical runs that end in 2005.

2.1. Observational data sets

The observational records for SAT and precipitation were obtained from two data sets, Climate Research Unit (CRU) TS v.3.22 (Harris *et al.*, 2014) and University of Delaware (UDEL) v.2.01 (Matsuura and Willmott, 2009). In addition, for precipitation we use the Global Precipitation Climatology Centre (GPCC) full v.6 (Schneider *et al.*, 2011; Schneider *et al.*, 2014). All data sets contain monthly land station records (mean SAT or total precipitation) that are quality controlled, and provided on a $0.5^\circ \times 0.5^\circ$ latitude/longitude grid. Emphasis is placed on GPCC for precipitation as it has the largest number of contributing gauge-based observations (>67 200 worldwide) (Schneider *et al.*, 2014). Juarez *et al.* (2009) compared GPCC precipitation with several other data sets over the tropical South America and showed reasonable agreement in precipitation between the data sets.

2.2. Model data sets

To assess the unforced variability of the climate system and its response to natural or anthropogenic forcing, we use the output of a 14-member subset of global climate models participating in the CMIP5 project. For each model (Table 1), we select one pre-industrial run, in which the atmospheric concentrations of all well-mixed greenhouse gases are held at pre-industrial levels. The pre-industrial simulations include an unperturbed land-use component and non-evolving emission and concentration of natural aerosols. Our hypothesis is that the distributions of temperature and precipitation trends during 30 and 50-year period of these natural-only simulations can provide an estimate of the variability of the climate system in the absence of external forcings. We also analyse historical simulations where external forcings are based on observed time-evolving data. The forcings in this case include a

variable atmospheric composition (including greenhouse gases) due to both anthropogenic and volcanic influences; solar forcing; land use; emissions or concentrations of short-lived species, and natural and anthropogenic aerosols or their precursors. The historical simulations span the period 1850–2005 (or longer) and allow us to discuss model performance against observed climate change in recent decades. Finally, for some models, we use the output from a natural-only run, which only includes natural forcing (i.e. volcanoes and solar variability). Table 1 gives further details on models and runs.

As a preliminary step, the output of the CMIP5 models was interpolated to the same grid as the observational data sets ($0.5^\circ \times 0.5^\circ$ latitude/longitude grid). Annual and seasonal means were calculated for each grid point. In the following, seasons will be named according to the Southern Hemisphere [December–February (DJF) – summer, March–May (MAM) – fall, June–August (JJA) – winter, and September–November (SON) – spring].

2.3. Methodology

The methodology employed in this study closely follows that used in detection and attribution analysis for the Mediterranean region by Barkhordarian *et al.* (2012, 2013). We start by performing a least squares fit to calculate the linear trends over the selected 30- and 50-year period for SAT and precipitation, respectively. Trends are weighted by the areal average of each grid cell, as a function of latitude, as are trends averaged over sub-regions (e.g. over Brazil, La Plata Basin, or the entire continent).

The significance of trends is tested against the null hypothesis that they arise from unforced variability alone, as estimated on the basis of the CMIP5 pre-industrial control runs. To estimate the distribution of trends in temperature (precipitation) in an unforced climate, we use the results from these pre-industrial runs for 166 (81) non-overlapping 30-year for SAT (50-year for precipitation) windows for a total of 4980 (4050) years (Table 1). We say that a trend, in either an observational or model data set, is significant when its p value is <0.05, i.e. when the trend is bigger (or smaller) than 95% of the trends derived from the pre-industrial control runs.

After testing significance in the observed trends, we compare them with those obtained from the CMIP5 models' historical runs. Each model may contain more than one ensemble per historical simulation, the difference among them being the initial conditions and physics imposed. In this article, we only use one ensemble per model. Trends are computed for individual models and the multi-model ensemble mean, together with the standard deviation of the sampling distribution of this mean,

$$\sigma_{\text{mean}} = \frac{\sigma}{\sqrt{n}} \tag{1}$$

where σ is the intra-model standard deviation and n is the number of models.

We say that a trend obtained from the observational data sets for a given variable, region, season, and period agrees with that in the multi-model ensemble of simulations if the difference between trends can be explained by the unforced variability of the climate system and the ensemble mean variance. That is, we consider agreement if,

$$\begin{aligned} &\left(\mu_{\text{obs}} + p_{5\%}, \mu_{\text{obs}} + p_{95\%}\right) \\ &\cap \left(\mu_{\text{model}} - \sigma_{\text{model}}, \mu_{\text{model}} + \sigma_{\text{model}}\right) \neq \emptyset \end{aligned} \tag{2}$$

where μ_{obs} is the observed trend, and $p_{5\%}$ ($p_{95\%}$) is the 5th (95th) percentile in the distribution of the trends derived from the pre-industrial control runs. So $(\mu_{\text{obs}} + p_{5\,\%}, \mu_{\text{obs}} + p_{95\,\%})$ approximately represents the 90% confidence interval of the forced trend (taking into account the unforced variability as an estimate from the pre-industrial control run). μ_{model} and σ_{model} are the mean and standard deviation of trends from multiple models. Illustration of Equation (2) is shown later in Figure 4. In the same way, we assess the agreement in trends between observation and a multi-model ensemble of the natural-only runs, where only natural forcings (e.g. volcanoes and solar variability) are taken into account.

Furthermore, we compare the spatial patterns of observed and simulated trends in SAT and precipitation. For this comparison, we use two parameters as evaluation metrics, the pattern correlation coefficient and model's biases normalized by spatially averaged trends in observation. The pattern correlation coefficient is given by

$$\frac{\sum \omega_{(i,j)} \cdot \left(\text{proj}_{(i,j)} - \acute{\text{p}}\text{roj}\right) \cdot \left(\text{obs}_{(i,j)} - \text{os}\right)}{\sqrt{\omega_{(i,j)\cdot} \left(\text{proj}_{(i,j)} - \acute{\text{p}}\text{roj}\right)^2} \cdot \sqrt{\omega_{(i,j)\cdot} \left(\text{obs}_{(i,j)} - \text{b}'\right)^2}} \tag{3}$$

where $\text{proj}_{(i,j)}$ and $\text{obs}_{(i,j)}$ are the simulated and observed trends at a grid point (i and j) respectively, $\overline{\text{proj}}$ and $\overline{\text{obs}}$ are their mean and $\omega_{(i,j)}$ is a weight function that accounts for the difference in grid-box size as a function of latitude. With the same notation, the normalized difference is given by

$$\frac{\overline{\text{proj}} - \overline{\text{obs}}}{\overline{\text{obs}}} \tag{4}$$

In what follows, SAT trends are presented for the entire South American continent and for Brazil. Precipitation trends are also presented for the entire continent, and for the southern part of the Plata Basin, which is defined as the land region north of 37°S, south of 23.5°S and east of 60°W. Our reasons for this choice of regions are given in the following section.

3. Results

3.1. Surface air temperature

Trends in annual mean SAT for the period 1975–2004 from CRU and UDEL over South America are shown in Figure 1. Stippling indicates grid points where the trend is significant according to the criteria defined in Section 2. The results obtained with the two data sets broadly agree in sign, magnitude, and significance. A significant warming

Table 1. The 14 CMIP5 models used in this study along with the number of years of control runs used to estimate the unforced variability of temperature (precipitation) trends.

Model	References	Pre-industrial run (years)	Historical run	Natural-only run
ACCESS1-0	Bi *et al.* (2013)	480 (400)	√	–
BCC-CSM1-1	Wu *et al.* (2014)	480 (350)	√	√
BNU-ESM	Ji *et al.* (2014)	540 (550)	√	√
CANESM2	Flato *et al.* (2000)	630 (450)	√	√
CCSM4	Gent *et al.* (2011)	–	√	–
MRI-CGM3	Yukimoto *et al.* (2011)	–	√	–
CNRM-CM5	Voldoire *et al.* (2013)	150 (–)	√	√
CSIRO-Mk3-6-0	Rotstayn *et al.* (2010)	–	√	–
GISS-E2-R	Miller *et al.* (2014)	–	√	–
INMCM4	Volodin *et al.* (2010)	480 (450)	√	–
IPSL-CM5A	Dufresne *et al.* (2013)	900 (950)	√	√
MIROC5	Watanabe *et al.* (2010)	540 (300)	√	–
MPI-ESM	Marsland *et al.* (2003)	780 (600)	√	–
NORESM1	Bentsen *et al.* (2013)	–	√	–

The types of runs, historical or natural-only, performed by each model are also displayed.

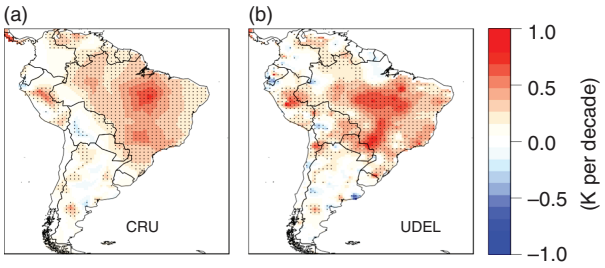

Figure 1. Annual mean SAT trends (K per decade) over South America for the period 1975–2004 as obtained from the CRU (a) and UDEL data sets (b). The dots indicate regions where the trend is significant.

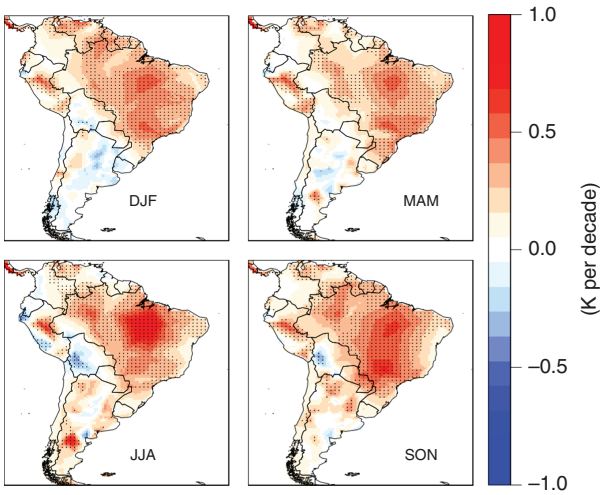

Figure 2. Seasonal mean SAT trends (K per decade) over South America for the period 1975–2004 from the CRU data set. The dots indicate regions where the trend is significant at the 95% confidence level.

trend is apparent over most of Brazil as well as over parts of Venezuela and Peru, with a maximum warming over north-central Brazil. Significant trends over the Guianas are present only in the CRU data set, while trends over Bolivia and Paraguay are present only in UDEL. These warming trends are in agreement with the IPCC AR5 (Magrin *et al.*, 2014) that indicates warming has been detected throughout South America since the mid-1970s. Cooling trends can be observed over western Bolivia and some regions in northern Patagonia. The patterns in the seasonal mean trends of SAT are very similar to those in the annual mean (Figure 2). We note that the maximum warming over north-central Brazil is more pronounced in the winter season (from June through August). This season is also characterized by a significant cooling trend over western Bolivia and the Pacific coast of Peru. In view of these results, we also consider the SAT trends over Brazil separately. Figure 3 shows the evolution of 30-year trends in the region for the period of 1902–2013. In the annual mean, temperature has been increasing for almost the entire period, but the warming trend becomes significant after 1968 (block 1968–1997), indicating a possible external forcing exerted. This same pattern is present in both the summer and winter seasons. As shown in Figure 2, the overall warming trend in Brazil is greatest in winter (JJA).

We next assess the agreement of the observed trends in SAT with those in the CMIP5 simulations. Figure 4 shows the seasonal and annual mean trends in observation (together with the estimation of the unforced variability), the CMIP5 historical simulations, and the CMIP5 natural-only simulations. For the entire South American continent, the multi-model ensemble of historical runs reproduces the observed trends very well with reasonable agreement in all seasons taking in account the unforced variability (red whiskers in Figure 4). In the case of the natural-only runs, the models exhibit a much weaker warming trend. For Brazil, the multi-model ensemble historical runs show warming in all seasons. However, the models consistently underestimate the observed warming with differences larger than the uncertainty in observed trends. There is no clear agreement among the

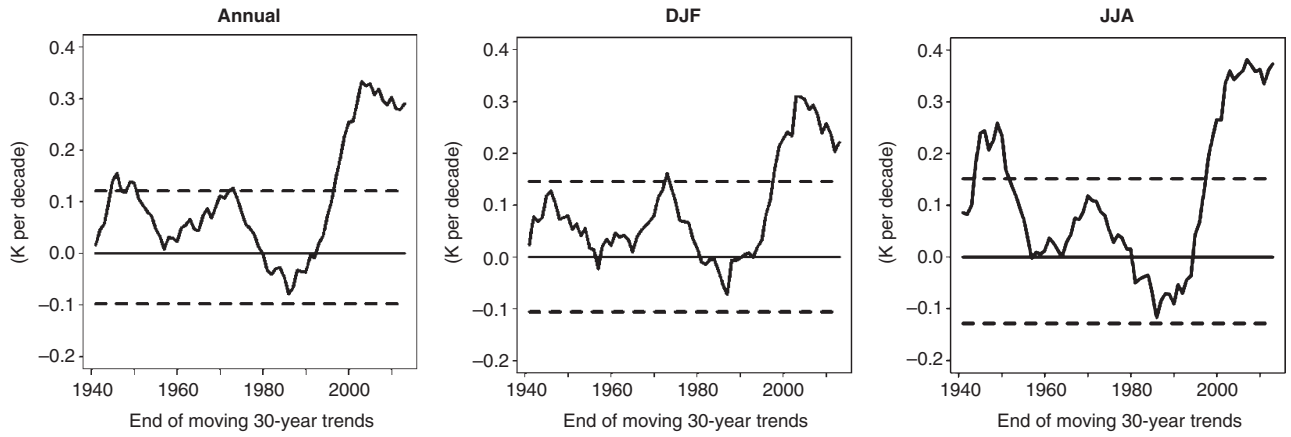

Figure 3. Moving 30-year temperature trends in the CRU dataset over Brazil for annual, DJF, and JJA. The year indicates the end of a 30-year block. The dashed lines indicate the 5th and 95th percentiles of trends estimated from the pre-industrial control runs.

natural-only runs and observations in any season, indicating that anthropogenic forcing is essential for CMIP5 models to reproduce the observed SAT trends over South America.

Figure 5 shows the point-wise agreement between observations and CMIP5 ensemble members over South America. Shading indicates the number of CMIP5 models (out of 14) whose SAT trends agree with observations to within the uncertainty range of unforced variability. Most models capture the trends in most regions, as indicated by the predominance of green shading. The biggest exception is for a region over north-central Brazil where the observed strong warming trend is not captured by the models. Additionally, some small regions in western Bolivia and over the Pacific coast of Peru, Chile, Ecuador, and Colombia show poor agreement. This brings us to an important point that the future SAT projection of CMIP5 models in these regions may underestimate trends under a changing climate.

The individual performance of each model can be summarized by its ability to represent the spatially averaged warming trends and the warming patterns over the continent. Figure 6 shows the spatial correlation coefficients and the differences in the mean trend between the observational data, historical simulations, and natural-only simulations. The differences are normalized by the spatially averaged trends in the observation. In 10 of the 14 CMIP5 historical runs examined, the magnitude of the differences from observed trends are within the uncertainty range of the unforced variability, which we interpret as having good agreement with observations. On the other hand, all five natural-only runs underestimate observations and the differences lie outside the range of unforced variability. Five models (ACCESS1-0, MRI-CGM3, GISS-E2-R, MIROC5, and MPI-ESM) stand out in capturing the warming pattern, with a higher correlation coefficient, as can be seen by their correct prediction of a maximum warming over Brazil (Figure 7). Two models (BNU-ESM and CNRM-CM5), on the other hand, are negatively correlated with observations, with a maximum warming in the southern part of the continent.

3.2. Precipitation

Figure 8 compares precipitation trends over the period 1955–2004 for the three observational data sets (CRU, UDEL, and GPCC). In all cases, a significant positive trend is apparent over a region that roughly encompasses the southern part of La Plata Basin (southern Brazil, Uruguay, and northeastern Argentina). While the trends over Patagonia are small, they are significant primarily because the climatological intra-seasonal variability in precipitation over this region is relatively small. Positive significant trends are also found in parts of Colombia, Ecuador, a region between Brazil, Guiana, and Venezuela, and a region between Brazil, Peru, and Bolivia. Negative significant trends are observed in all data sets over southern Chile and French Guiana. Similar to Rao *et al.* (2015), which studied precipitation trends over Brazil for the period 1979–2011, we find significant negative trends over regions in central and northern Brazil (GPCC and UDEL) and along the border between Brazil and Venezuela (all three data sets), as well as significant positive trends in western NEB (CRU) and in the border between Brazil and Peru (CRU and UDEL).

Unlike SAT in Figure 2, the magnitude and signs of the trends vary depending on season (Figure 9). The positive trends over the southern Plata Basin are stronger in the austral fall (MAM) and spring (SON), while negative trends appear in winter (JJA). Even though these winter trends are weaker than in any other season, they are significant over almost the entire continent due to the weak variance in precipitation during this season. In the fall, we find positive significant trends north of the equator in Colombia, Venezuela, and Guiana, but no significant trends in the other seasons. Another interesting feature is that the negative trends over the Amazon Basin are stronger during spring, in accordance with Espinoza Villar *et al.* (2009). Finally, in summer (DJF), there are significant positive trends in many regions of Peru, Bolivia, Argentina, Uruguay, and Brazil with large spatial variability.

Narrowing down on the southern Plata Basin where the trends are strongest and regionally homogeneous,

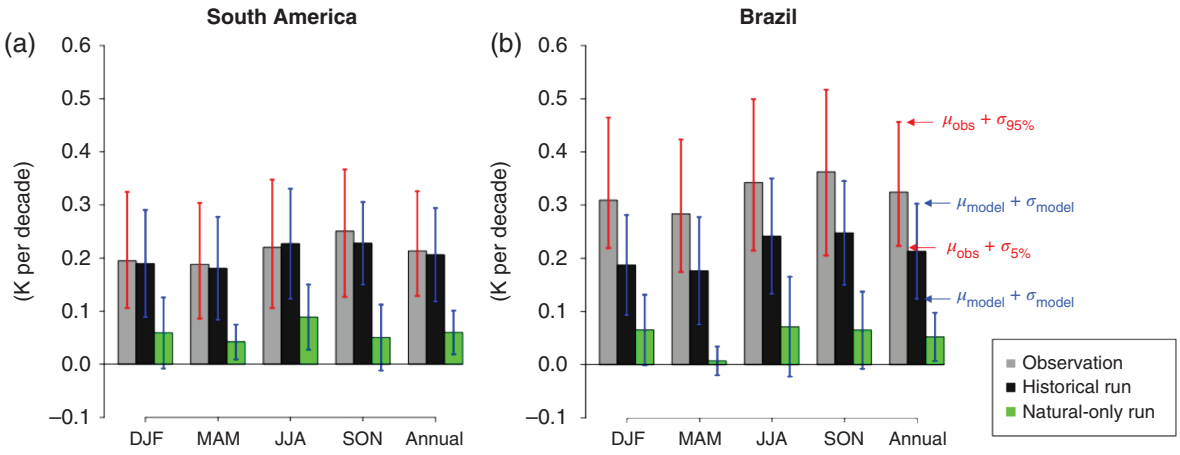

Figure 4. Temperature trends (K per decade) over (a) South America and (b) Brazil for the period 1975–2004. The light grey bar represents the observed trends (average between the two data sets, CRU and UDEL). The dark grey bar represents the predictions from 14 models that take into account the historical forcings (anthropogenic and natural). The green bar represents the predictions (from five models) using only natural forcings. The red whiskers represent the 90% confidence interval of the unforced variability as estimated from the pre-industrial control runs. The blue whiskers represent the standard deviation of the trends across multiple models for each experiment.

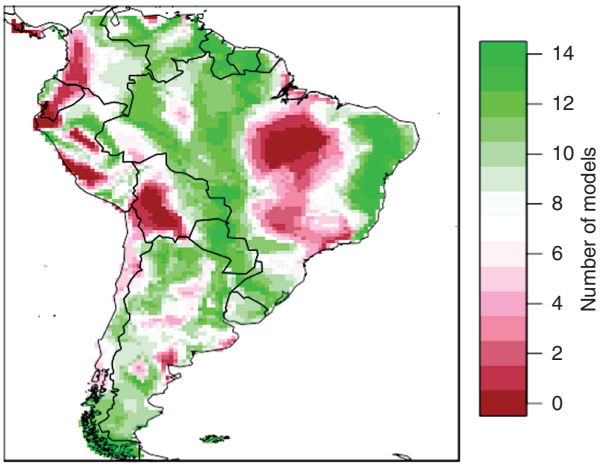

Figure 5. Agreement between the trends in the observation and in the predictions by different models with historical forcing for the period of 1975–2004. The plot represents the number of models that agrees with observations, within the uncertainty range of the unforced variability.

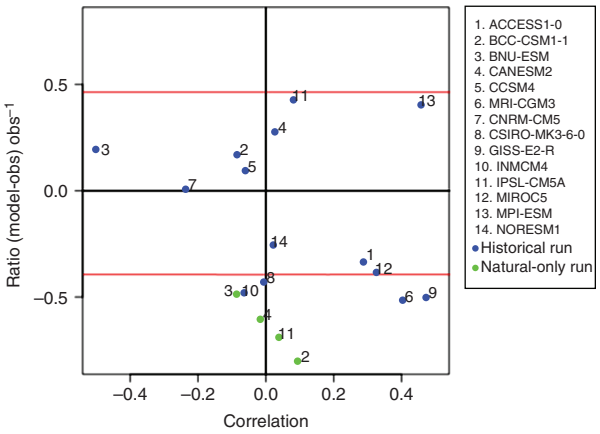

Figure 6. Individual performance of models in the historical and natural-only runs for the annual mean SAT over the South American continent. The performance is measured by the pattern correlation coefficients between observed and simulated trends, and the normalized biases of the models. The two red lines indicate the 5th and 95th percentiles of trends as estimated from the pre-industrial control runs. The CNRM-CM5 natural-only run, not shown in the figure, has a ratio of −0.99 and correlation of −0.32.

Figure 10 reveals that the 50-year trends in annual precipitation have been significant during the second half of the last century. There are, however, considerable seasonal variations. Trends in summer are consistently positive over the period (Figure 10); however, values are significant only during 1960–1975 and 1995–2005. Positive trends in precipitation over La Plata Basin, especially in its southern part, have been related to the increase in streamflow of the main rivers of the region (Genta *et al.*, 1998; Barros *et al.*, 2005; Doyle and Barros, 2011). Trends in winter are also positive over almost all of the last century, but they are significant mostly in the period 1980–2000 after which they reverse sign (Figure 10). The recent decrease in wintertime precipitation of >1 mm month^{-1} per decade is significant compared to those from the pre-industrial control simulations.

Figure 11 shows the seasonal and annual mean trends in the observations and CMIP5 simulations over South America and southern Plata Basin together with an estimation of the unforced variability. Over the South American continent, the annual mean precipitation in the CRU and GPCC data sets exhibits an increasing trend that is significant only in the CRU (0.93 mm month^{-1} per decade). For this data set, we also find a significant increasing trend in precipitation for summer, fall, and spring (1.3, 1.3, and 1.1 mm month^{-1} per decade, respectively). No significant trends are obtained in winter. The multi-model ensemble of the historical runs underestimates the magnitude of the observed trends. Over the southern Plata Basin, all three observational data sets obtain a significant increase in annual mean precipitation (2.7 mm month^{-1} per decade in average) as well as in the seasonal mean for summer, fall, and spring (4.2,

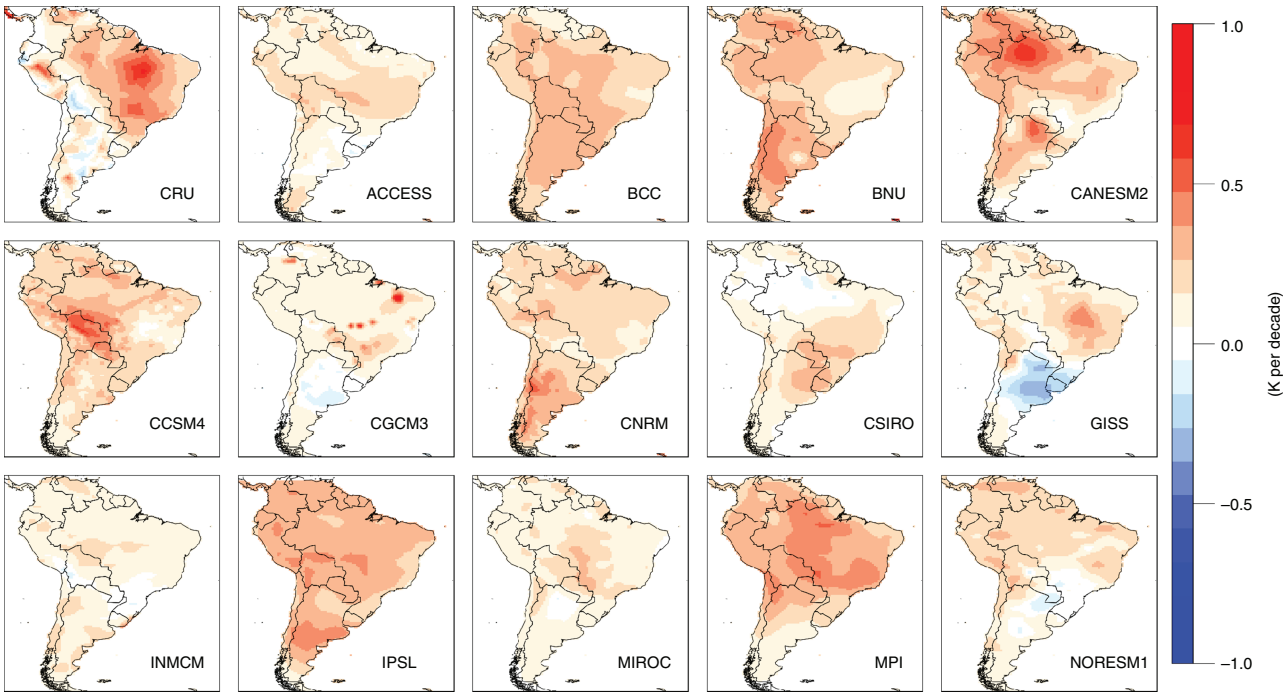

Figure 7. Annual mean SAT trends over South America for the period 1975–2004 as obtained from 14 CMIP5 models' historical runs and the CRU data set.

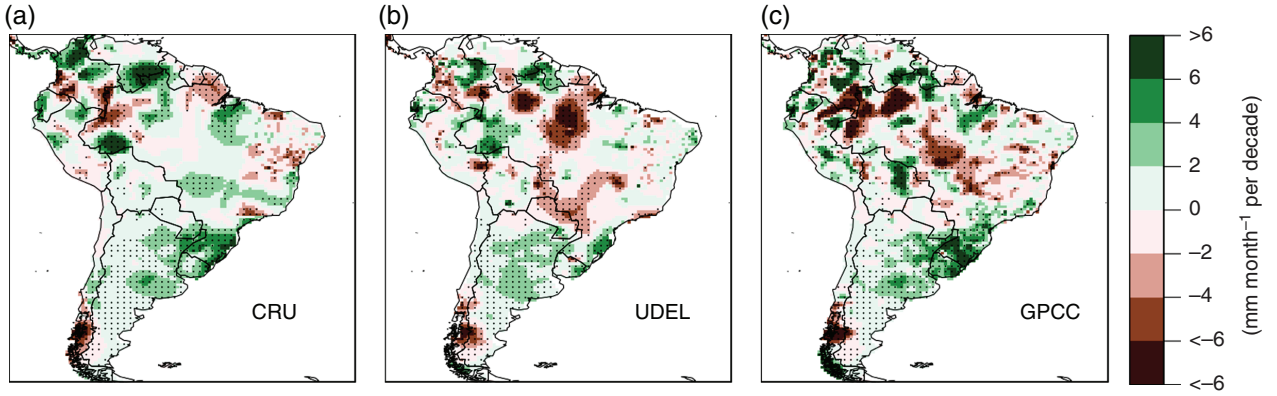

Figure 8. Monthly total precipitation trends (mm month^{-1} per decade) over South America for the period 1955–2004 as obtained from the CRU, UDEL, and GPCC data sets ((a)–(c), respectively). The dots indicate regions where the trend is significant at the 95% confidence level.

4.7, and 3.4 mm month^{-1} per decade, respectively). The CRU and UDEL data sets exhibit a significant decreasing trend during winter (−1.6 and −2.9 mm month^{-1} per decade, respectively). The multi-model ensemble of simulated trends from CMIP5 historical runs, however, does not show significant trends either in the annual mean or in any season.

Unlike SAT, it is hard to define precipitation trends representing the entire South American continent. This is primarily because precipitation trends at and near the Tropics are weaker than the unforced variability. Figure 12 shows the annual and season mean precipitation and trends from the GPCC data set for the period 1955–2004 over three latitude bands of South America representing the Tropics, subtropics, and extratropics (0°–15°S, 15°–30°S, and 30°–45°S, respectively). These three regions shown in Figure 12, exclude grid points that lie west of the Andes, where higher spatial resolutions than CMIP5 models is required to simulate realistic precipitation and its trends. The annual mean precipitation generally decreases from north to south. The tropical and subtropical bands show minimum precipitation during winter and maximum during summer, while the extratropical band does not have clear wet and dry seasons. The annual mean precipitation over the period 1955–2004 shows a decreasing trend over the tropical band and an increasing trend over the subtropical band, none of which is significant. The only significant trends in precipitation can be found in the extratropical band; these trends are positive except during winter. Therefore, there is considerable uncertainty in the observed precipitation trends over the Tropics and subtropics in South America. The trend over the extratropics is significant in the observations for all seasons.

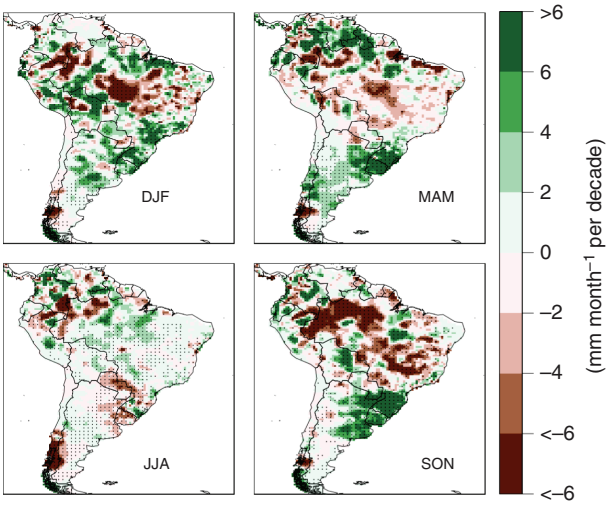

Figure 9. Seasonal mean GPCC precipitation trends (mm month^{-1} per decade) over South America for the period 1955–2004. The dots indicate regions where the trends are significant.

4. Conclusions

Using two observational data sets, our study finds that SAT has been increasing over much of South America during the period 1975–2004, which is in line with IPCC AR5. Unlike previous studies, we quantified uncertainty of the observed trends by comparison with those obtained in pre-industrial CMIP5 simulations. From the CMIP5 simulations with natural-only forcing, we find that this overall warming over the continent cannot be explained by natural climate variability alone. Moreover, the historical CMIP5 simulations with both natural and anthropogenic forcing reproduce the observed warming trends with reasonable fidelity. These results suggest that anthropogenic warming is already evident over much of South America.

The warming detected is particularly strong over most of Brazil where values up to 1 K decade^{-1} are obtained. However, simulated warming trends show some discrepancies at the regional level. Trends in CMIP5 historical simulations are systematically weaker than in the observations over central Brazil, and substantially different from the observations over the western part of the continent. Over much of southern and northern South America trends are relatively weak. In regions where some models simulate observed warming trends well, confidence can be boosted in future projections of temperature by the models. Similarly, in regions where models show considerable disagreement with observations regarding warming trends, caution might be exercised in interpreting future projections. The entire South American continent is an example of the former regions and central Brazil is an example of the latter. However, natural variability contributes substantial uncertainty to projected temperature trends on local, regional, and continental scale (Deser *et al.*, 2012).

Trends in precipitation over the period 1955–2004 are found to be much less spatially coherent, with many sign changes over relatively short distances. None of the observation data sets show significant trends in precipitation averaged over the entire South American continent. Over an extratropical region that roughly encompasses the southern part of La Plata Basin (southern Brazil, Uruguay, and northeastern Argentina), all observational data sets show significant trends compared to unforced natural variability. The historical CMIP5 simulations do not capture this feature. It is well known that CMIP5 models project an overall decrease in precipitation over the subtropics and an overall increase in precipitation over the Tropics and mid to high latitudes by the end of the 21st century. Our observational data sets for a recent period reproduce this feature with significance only over mid to high latitudes. This emphasizes the importance of taking regional precipitation characteristics into account for predictions of a changing future climate.

Thus, while anthropogenic global warming is being detected in the temperature record, the effects on precipitation have yet to emerge from the noise in most locations in South America. The spatial inhomogeneity of the precipitation trends, which is largely influenced by orography and large-scale circulation, provides a difficult

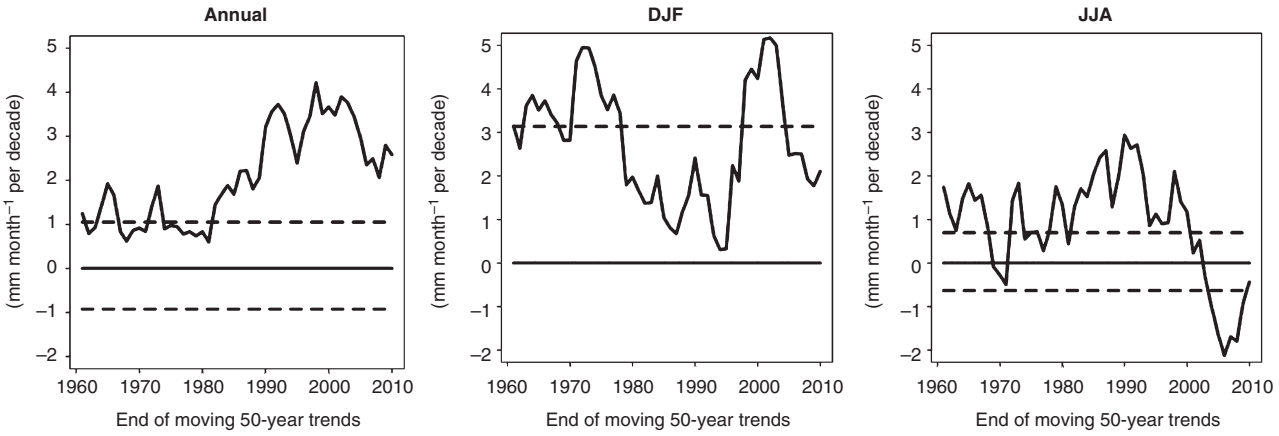

Figure 10. Moving 50-year precipitation trends over the southern part of the Plata Basin for the annual and seasonal means, obtained from the GPCC data set. The years in the x-axis indicate the end of a 50-year block. The dashed lines indicate the 5th and 95th percentiles of trends estimated from the pre-industrial control runs.

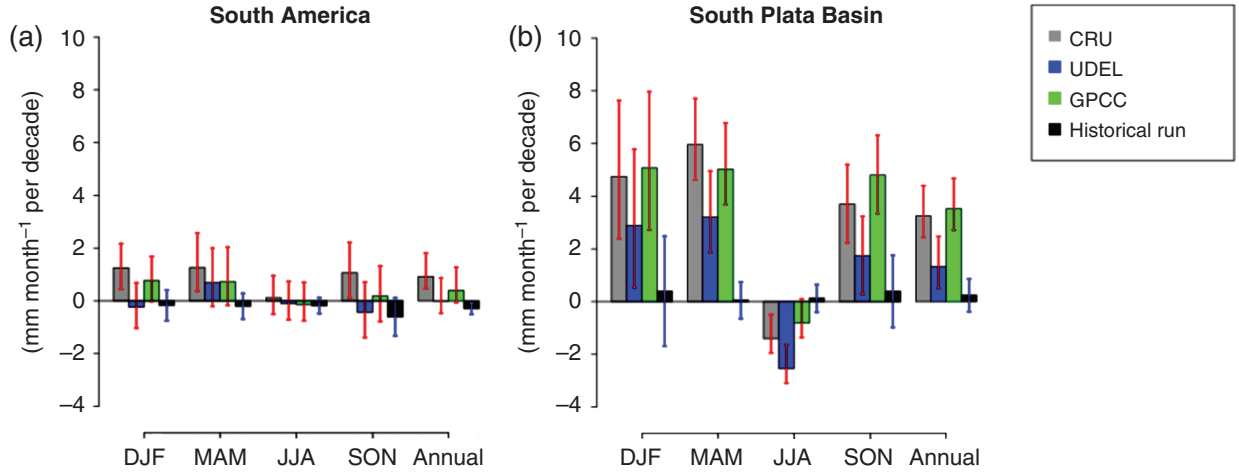

Figure 11. Precipitation trends (mm month^{-1} per decade) over (a) South America and (b) South Plata Basin for the period 1955–2004. The light grey, blue, and green bars represent the observed trends as calculated from the CRU, UDEL, and GPCC data sets, respectively. The black bar represents the trends from 13 models that take into account the historical forcings (anthropogenic and natural). The red whiskers represent the unforced variability as estimated from the pre-industrial control runs. The blue whiskers represent the standard deviation of the trends across the multiple models for each experiment.

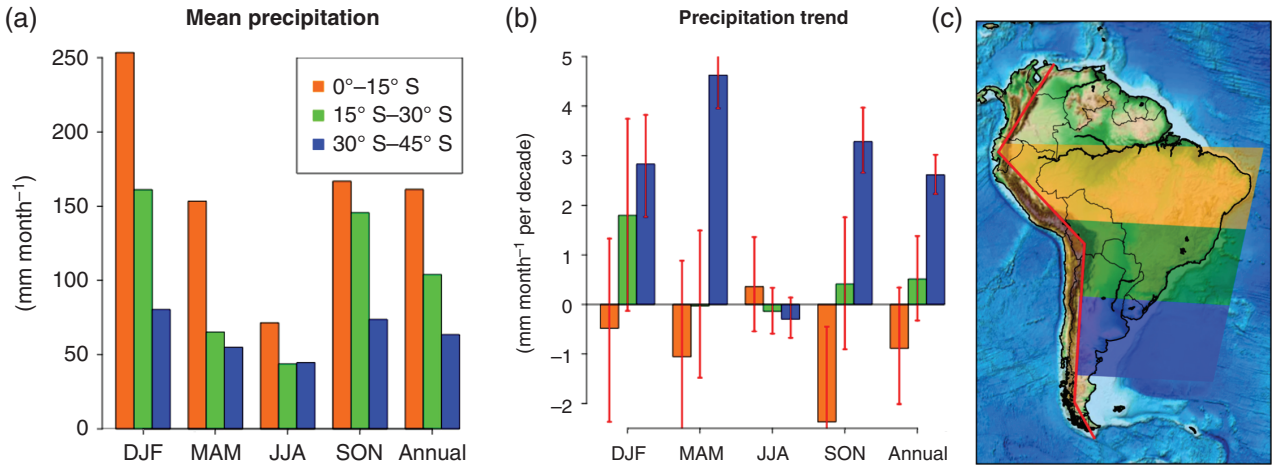

Figure 12. Precipitation mean (a) and trends (b) over three latitude bands of South America, 0°–15°S, 15°–30°S, and 30°–45°S, for the period 1955–2004, as obtained from the GPCC data set over land excluding grid points west of the Andes as displayed on the map (c). The red whiskers represent the unforced variability as estimated from the pre-industrial control runs.

target for assessing model fidelity. The skill in reproducing the mean precipitation climatology can offer some background on whether the CMIP5 models have the capability to simulate future changes in precipitation with success. Model success varies considerably across the CMIP5 ensemble (see Supporting Information). Although most models capture a precipitation maximum over Amazonia and a minimum over the southern portion of the continent in austral summer, one cannot claim overall success in the simulation of the American monsoon system.

This study raises several questions. Will the regions that have experienced the greatest warming continue to warm more rapidly than other regions? Will the regions that have not experienced significant warming begin to warm (or cool) in the coming decades? What is the role of low-frequency large-scale climate variability (e.g. remote SST forcing) in the magnitude of observed trends? For precipitation, further investigation into regional changes, changes in the seasonal cycle, and connecting observed changes with mechanisms would shed more light on the meaning of the results presented here. Such work would be a logical next step in understanding what effect if any, anthropogenic climate forcing has had on precipitation over South America *versus* what component of the observed trends is a result of low-frequency climate variability.

We end by emphasizing that our analysis relies on a significant and somewhat controversial assumption, namely that the magnitude of the natural climate variability as described by CMIP5 pre-industrial simulations is realistic. The robustness of the detection results, henceforth, is subject to models correctly simulating natural climate variability. It is now recognized that models may underestimate modes of climate variability such as the El Niño Southern Oscillation, which has strong climate impacts over South America (Kumar *et al.*, 2013; Chadwick *et al.*,

2015). This underestimation may lead to spurious detection results, if as a consequence the simulated natural variability is of smaller amplitude than the real variability. In addition, we find significant results, particularly in precipitation, for a relative small region such as La Plata Basin where global climate models have few grid points. We assign confidence to these results due to the several studies with observational data for the regions that agree with our findings.

Acknowledgements

Partial support at University of California Los Angeles was provided by the US Department of Energy under the GoAmazon2014/5 programme. Support was provided by the US National Science Foundation AGS-1547899. The contribution by H.L. to this study was carried out on behalf of the Jet Propulsion Laboratory, California Institute of Technology, under a contract with the National Aeronautics and Space Administration.

Supporting information

The following supporting information is available as part of the online article:

Figure S1. Precipitation climatology for the austral summer (DJF) over South America for the period 1955–2004 as obtained from GPCC, CRU, and 13 CMIP5 models' historical simulations.

Figure S2. Taylor diagram displaying the performance of the summer mean precipitation climatology in CMIP5 historical simulations against observation, obtained from the GPCC data set, for the period 1955–2004 over South America.

Figure S3. Standard deviation of monthly precipitation over a year, obtained by using the GPCC data set; mean value for the period 1955–2004 (left); and linear trend for the period 1955–2004 (right).

Figure S4. Standardized anomaly of the monthly total precipitation for the period 1955–2004 (5-year mean), as obtained from the GPCC data set. Nordeste (left) and South Plata Basin (right).

References

Arias PA, Fu R, Hoyos CD, Li WH, Zhou LM. 2011. Changes in cloudiness over the Amazon rainforests during the last two decades: diagnostic and potential causes. *Clim. Dyn.* **37**: 1151–1164, doi: 10.1007/s00382-010-0903-2.

Barkhordarian A, Bhend J, von Storch H. 2012. Consistency of observed near surface temperature trends with climate change projections over the Mediterranean region. *Clim. Dyn.* **38**: 1695–1702.

Barkhordarian A, von Storch H, Bhend J. 2013. The expectation of future precipitation change over the Mediterranean region is different from what we observe. *Clim. Dyn.* **40**: 225–244, doi: 10.1007/s00382-012-1497-7.

Barros V, Doyle M, Camilloni I. 2005. Potential impacts of climate change in the Plata basin. Regional hydrological impacts of climatic variability and change. In *Proceedings of Symposium S6 Held during the Seventh IAHS Scientific Assembly at Foz do Iguaçu*, Brazil, April 2005, IAHS Publ. 295.

Bentsen M, Bethke I, Debernard JB, Iversen T, Kirkevag A, Seland O, Drange H, Roelandt C, Seierstad IA, Hoose C, Kristjansson JE. 2013. The Norwegian Earth System Model, NorESM1-M – Part 1: Description and basic evaluation of the physical climate. *Geosci. Model Dev.* **6**: 687–720, doi: 10.5194/gmd-6-687-2013.

Bi D, Dix M, Marsland S, OFarrell S, Rashid H, Uotila P, Hirst A, Kowalczyk E, Golebiewski M, Sullivan A, Yan H, Hannah N, Franklin C, Sun Z, Vohralik P, Watterson I, Zhou X, Fiedler R, Collier M, Ma Y, Noonan J, Stevens L, Uhe P, Zhu H, Griffies S, Hill R, Harris C, Puri K. 2013. The ACCESS coupled model: description, control climate and evaluation. *Aust. Meteorol. Ocean.* **63**: 41–64.

Bradley RS, Keimig FT, Diaz HF, Hardy DR. 2009. Recent changes in freezing level heights in the Tropics with implications for the deglacierization of high mountain regions. *Geophys. Res. Lett.* **36**: L17701, doi: 10.1029/2009gl037712.

Chadwick R, Good P, Martin G, Rowell DP. 2015. Large rainfall changes expected over tropical land in the coming century. *Nat. Clim. Change*. (in press).

Deser C, Phillips A, Bourdette V, Teng H. 2012. Uncertainty in climate change projections: the role of internal variability. *Clim. Dyn.* **38**: 527–546, doi: 10.1007/s00382-010-0977-x.

Doyle ME, Barros VR. 2011. Attribution of the river flow growth in the Plata Basin. *Int. J. Climatol.* **31**: 2234–2248, doi: 10.1002/joc.2228.

Dufresne JL, Foujols MA, Denvil S, Caubel A, Marti O, Aumont O, Balkanski Y, Bekki S, Bellenger H, Benshila R, Bony S, Bopp L, Braconnot P, Brockmann P, Cadule P, Cheruy F, Codron F, Cozic A, Cugnet D, de Noblet N, Duvel JP, Ethe C, Fairhead L, Fichefet T, Flavoni S, Friedlingstein P, Grandpeix JY, Guez L, Guilyardi E, Hauglustaine D, Hourdin F, Idelkadi A, Ghattas J, Joussaume S, Kageyama M, Krinner G, Labetoulle S, Lahellec A, Lefebvre MP, Lefevre F, Levy C, Li ZX, Lloyd J, Lott F, Madec G, Mancip M, Marchand M, Masson S, Meurdesoif Y, Mignot J, Musat I, Parouty S, Polcher J, Rio C, Schulz M, Swingedouw D, Szopa S, Talandier C, Terray P, Viovy N, Vuichard N. 2013. Climate change projections using the IPSL-CM5 Earth System Model: from CMIP3 to CMIP5. *Clim. Dyn.* **40**: 2123–2165, doi: 10.1007/s00382-012-1636-1.

Espinoza Villar JC, Ronchail J, Guyot JL, Cochonneau G, Naziano F, Lavado W, de Oliveira E, Pombosa R, Vauchel P. 2009. Spatio-temporal rainfall variability in the Amazon basin countries (Brazil, Peru, Bolivia, Colombia, and Ecuador). *Int. J. Climatol.* **29**: 1574–1594.

Exbrayat JF, Williams M. 2015. Quantifying the net contribution of the historical Amazonian deforestation to climate change. *Geophys. Res. Lett.* **42**: 2968–2976, doi: 10.1002/2015gl063497.

Flato GM, Boer GJ, Lee WG, McFarlane NA, Ramsden D, Reader MC, Weaver AJ. 2000. The Canadian Centre for Climate Modelling and Analysis global coupled model and its climate. *Clim. Dyn.* **16**: 451–467, doi: 10.1007/s003820050339.

Fu R, Yin L, Li W, Arias PA, Dickinson RE, Huang L, Chakraborty S, Fernandes K, Liebmann B, Fisher R, Myneni RB. 2013. Increased dry-season length over southern Amazonia in recent decades and its implication for future climate projection. *Proc. Natl. Acad. Sci. U.S.A.* **110**: 18110–18115, doi: 10.1073/pnas.1302584110.

Gent PR, Danabasoglu G, Donner LJ, Holland MM, Hunke EC, Jayne SR, Lawrence DM, Neale RB, Rasch PJ, Vertenstein M, Worley PH, Yang ZL, Zhang M. 2011. The Community Climate System Model Version 4. *J. Clim.* **24**: 4973–4991, doi: 10.1175/2011jcli4083.1.

Genta J, Perez-Iribarren G, Mechoso CR. 1998. A recent increasing trend in the streamflow of rivers in southeastern South America. *J. Clim.* **11**: 2858–2862.

Harris I, Jones PD, Osborn TJ, Lister DH. 2014. Updated high-resolution grids of monthly climatic observations – the CRU TS3.10 dataset. *Int. J. Climatol.* **34**: 623–642, doi: 10.1002/joc.3711.

IPCC. 2013. *Climate Change 2013: The Physical Science Basis. Contribution of Working Group I to the Fifth Assessment Report of the Intergovernmental Panel on Climate Change*. Cambridge University Press: Cambridge, UK and New York, NY, 1535 pp.

Ji D, Wang L, Feng J, Wu Q, Cheng H, Zhang Q, Yang J, Dong W, Dai Y, Gong D, Zhang RH, Wang X, Liu J, Moore JC, Chen D, Zhou M. 2014. Description and basic evaluation of Beijing Normal University Earth System Model (BNU-ESM) version 1. *Geosci. Model Dev.* **7**: 2039–2064, doi: 10.5194/gmd-7-2039-2014.

Juarez RIN, Li WH, Fu R, Fernandes K, Cardoso AD. 2009. Comparison of precipitation datasets over the tropical South American and African continents. *J. Hydrometeorol.* **10**: 289–299, doi: 10.1175/2008jhm1023.1.

Kayano MT, Andreoli RV. 2007. Relations of South American summer rainfall interannual variations with the Pacific Decadal Oscillation. *Int. J. Climatol.* **27**: 531–540, doi: 10.1002/joc.1417.

Knight JR, Folland CK, Scaife AA. 2006. Climate impacts of the Atlantic Multidecadal Oscillation. *Geophys. Res. Lett.* **33**: L17706, doi: 10.1029/2006GL026242.

Knutti R, Sedlacek J. 2013. Robustness and uncertainties in the new CMIP5 climate model projections. *Nat. Clim. Change* **3**: 369–373, doi: 10.1038/Nclimate1716.

Kumar S, Merwade V, Kinter JL III, Niyogi D. 2013. Evaluation of temperature and precipitation trends and long-term persistence in CMIP5 twentieth-century climate simulations. *J. Clim.* **26**: 4168–4185.

Lavado Casimiro WS, Ronchail J, Labat D, Espinoza JC, Guyot JL. 2012. Basin-scale analysis of rainfall and runoff in Peru (1969-2004): Pacific, Titicaca and Amazonas drainages. *Hydrol. Sci. J.* **57**: 625–642.

Magrin GO, Marengo JA, Boulanger JP, Buckeridge MS, Castellanos E, Poveda G, Scarano FR, Vicuna S. 2014. Central and South America. In *Climate Change 2014: Impacts, Adaptation, and Vulnerability. Part B: Regional Aspects. Contribution of Working Group II to the Fifth Assessment Report of the Intergovernmental Panel on Climate Change*, Barros VR, Field CB, Dokken DJ, Mastrandrea MD, Mach KJ, Bilir TE, Chatterjee M, Ebi KL, Estrada YO, Genova RC, Girma B, Kissel ES, Levy AN, MacCracken S, Mastrandrea PR, White LL (eds). Cambridge University Press: Cambridge, UK and New York, NY, 1499–1566.

Mantua N, Hare S. 2002. The Pacific Decadal Oscillation. *J. Oceanogr.* **58**: 35–44.

Marengo JA, Alves LM, Soares WR, Rodriguez DA, Camargo H, Riveros MP, Pablo AD. 2013. Two contrasting severe seasonal extremes in tropical South America in 2012: flood in Amazonia and drought in northeast Brazil. *J. Clim.* **26**: 9137–9154, doi: 10.1175/Jcli-D-12-00642.1.

Marsland SJ, Haak H, Jungclaus JH, Latif M, Roske F. 2003. The Max-Planck-Institute global ocean/sea ice model with orthogonal curvilinear coordinates. *Ocean Model.* **5**: 91–127, doi: 10.1016/S1463-5003(02)00015-X.

Matsuura K, Willmott C. 2009. Terrestrial air temperature and precipitation: 1900-2008 gridded monthly time series (V2.01). Center for Climatic Research, Department of Geography, University of Delaware. http://climate.geog.udel.edu/~climate/html_pages/archive.html (accessed 1 June 2015).

Mechoso CR, Iribarren GP. 1992. Streamflow in southeastern South-America and the Southern Oscillation. *J. Clim.* **5**: 1535–1539, doi: 10.1175/1520-0442(1992)005<1535:Sissaa>2.0.Co;2.

Meyer WB, Turner II BL (eds). 1994. Changes in land use and land cover: a global perspective. *Papers Presented at the 1991 OEIS Global Change Institute Conference, held in Snowmass Village, CO*. New York, NY: Cambridge University Press.

Miller RL, Schmidt GA, Nazarenko LS, Tausnev N, Bauer SE, Del Genio AD, Kelley M, Lo KK, Ruedy R, Shindell DT, Aleinov I, Bauer M, Bleck R, Canuto V, Chen YH, Cheng Y, Clune TL, Faluvegi G, Hansen JE, Healy RJ, Kiang NY, Koch D, Lacis AA, LeGrande AN, Lerner J, Menon S, Oinas V, García-Pando CP, Perlwitz JP, Puma MJ, Rind D, Romanou A, Russell GL, Sato M, Sun S, Tsigaridis K, Unger N, Voulgarakis A, Yao MS, Zhang J. 2014. CMIP5 historical simulations (1850-2012) with GISS ModelE2. *J. Adv. Model. Earth Syst.* **6**: 441–477, doi: 10.1002/2013ms000266.

Rao VB, Franchito SH, Santo CME, Gan MA. 2015. An update on the rainfall characteristics of Brazil: seasonal variations and trends in 1979-2011. *Int. J. Climatol.* **36**: 291–302, doi:10.1002/joc.4345.

Robertson AW, Mechoso CR. 1998. Interannual and decadal cycles in river flows of southeastern South America. *J. Clim.* **11**: 2570–2581, doi: 10.1175/1520-0442(1998)011<2570:IADCIR>2.0.CO;2.

Ropelewski CF, Halpert MS. 1987. Global and regional scale precipitation patterns associated with the El-Nino Southern Oscillation. *Mon. Weather Rev.* **115**: 1606–1626, doi: 10.1175/1520-0493(1987)115<1606:Garspp>2.0.Co;2.

Rotstayn LD, Collier AM, Dix MR, Feng Y, Gordon HB, Ofarrell SP, Smith IN, Syktus J. 2010. Improved simulation of Australian climate and ENSO-related climate variability in a GCM with an interactive aerosol treatment. *Int. J. Climatol.* **30**(7): 1067–1088.

Schneider U, Becker A, Finger P, Meyer-Christoffer A, Rudolf B, and Ziese M, 2011. GPCC Full Data Reanalysis Version 6.0 at 0.5°: Monthly Land-Surface Precipitation from Rain-Gauges Built on GTS-based and Historic Data, doi: 10.5676/DWD_GPCC/FD_M_V6_050.

Schneider U, Becker A, Finger P, Meyer-Christoffer A, Ziese M, Rudolf B. 2014. GPCC's new land surface precipitation climatology based on quality-controlled *in situ* data and its role in quantifying the global water cycle. *Theor. Appl. Climatol.* **115**: 15–40, doi: 10.1007/s00704-013-0860-x.

Taylor KE, Stouffer RJ, Meehl GA. 2012. An overview of Cmip5 and the experiment design. *Bull. Am. Meteorol. Soc.* **93**: 485–498, doi: 10.1175/Bams-D-11-00094.1.

Voldoire A, Sanchez-Gomez E, Salas y Melia D, Decharme B, Cassou C, Senesi S, Valcke S, Beau I, Alias A, Chevallier M, Deque M, Deshayes J, Douville H, Fernandez E, Madec G, Maisonnave E, Moine MP, Planton S, Saint-Martin D, Szopa S, Tyteca S, Alkama R, Belamari S, Braun A, Coquart L, Chauvin F. 2013. The CNRM-CM5.1 global climate model: description and basic evaluation. *Clim. Dyn.* **40**: 2091–2121, doi: 10.1007/s00382-011-1259-y.

Volodin EM, Dianskii NA, Gusev AV. 2010. Simulating present-day climate with the INMCM4.0 coupled model of the atmospheric and oceanic general circulations. *Izv. Atmos. Ocean. Phys.* **46**: 414–431, doi: 10.1134/S000143381004002x.

Watanabe M, Suzuki Y, Oishi R, Komuro Y, Watanabe S, Emori S, Takemura T, Chikira M, Ogura T, Sekiguchi M, Takata K, Yamazaki D, Yokohata T, Nozawa T, Hasumi H, Tatebe H, Kimoto M. 2010. Improved climate simulation by MIROC5. Mean states, variability, and climate sensitivity. *J. Clim.* **23**: 6312–6335, doi: 10.1175/2010jcli3679.1.

Wu T, Song L, Li W, Wang Z, Zhang H, Xin X, Zhang Y, Zhang L, Li J, Wu F, Liu Y, Zhang F, Shi X, Chu X, Zhang J, Fang Y, Wang F, Lu Y. 2014. An overview of BCC climate system model development and application for climate change studies. *J. Meteorol. Res.* **28**: 34–56, doi: 10.1007/s13351-014-3041-7.

Yukimoto S, Yoshimura H, Hosaka M, Sakami T, Tsujino H, Hirabara M, Tanaka TY, Deushi M, Obata A, Nakano H, Adachi Y, Shindo E, Yabu S, Ose T, Kitoh A. 2011. Meteorological Research Institute-Earth System Model Version 1 (MRI-ESM1) – model description. *Technical Report of the Meteorological Research Institute* 64.

Zhang XB, Zwiers FW, Stott PA. 2006. Multimodel multisignal climate change detection at regional scale. *J. Clim.* **19**: 4294–4307, doi: 10.1175/Jcli3851.1.

Zwiers FW, Zhang XB. 2003. Toward regional-scale climate change detection. *J. Clim.* **16**: 793–797, doi: 10.1175/1520-0442(2003)016<0793:Trsccd>2.0.Co;2.

